JOURNAL OF MATERIALS SCIENCE 30 (1995) 3782–3790

Crack growth and residual stress in Al–Li metal matrix composites under far-field cyclic compression

R. HERMANN
Materials Department, Faculty of Technology, The Open University, Milton Keynes MK7 6AA, UK

The growth of cracks under far-field cyclic compressive loading in aluminium–lithium (Al–Li) alloys reinforced with SiC particulates is investigated in notched compact tension specimens (CT). When cracks were initiated from the root of the notch, progressive deceleration occurred with the initial crack growth being largest. After crack arrest, analysis indicated that the initial residual stress diminished as the crack became non-propagating and at arrest the crack faces appeared to be open. When the crack closure loads were determined, it was shown that not all the stress amplitude produced crack growth and opening. This effect of crack closure was enhanced for small stress fields when the effective stress intensity dropped to the fatigue threshold of the alloy. For large residual stress fields the effective stress intensity range was well above the threshold and the initial crack growth rates were largest in the alloy containing the reinforcement particles. A residual strain model was used to determine the residual stress introduced in the root of the notch from the first compressive preload. It is shown that the fatigue crack growth was confined to a region of tensile stress within the residual stress field and the initial crack propagation rates were enhanced by the presence of the reinforcement. A dependence of the stress magnitude on growth rates was also established – the greater the residual stress at the root of the notch the larger the growth rates. The reinforcement had an additional "amplification" effect in terms of tensile distance from the notch. The effective stress intensity range, ΔK, was investigated using compliance measurements and a model is introduced which explains the underlying features and mechanism of accelerated growth in both alloys, taking into account the reinforcement phase, plastic zone-size dependence and the residual stress field of the MMC.

1. Introduction

In the recent past, Al–Li alloys (because of their lower density and higher stiffness) have been developed in air frame systems to replace the commonly used 2000 and 7000 series aluminium alloys. Al–Li alloys have yet to replace conventional aluminium alloys due to some unattractive fracture and fatigue behaviour. The first cause for concern with Al–Li–X alloy (AA 2020) was the low fracture toughness, K_{IC}, and the microstructural properties which affected this alloy [1].

Like conventional aluminium alloys, Al–Li alloy fracture behaviour, in particular K_{IC}, is affected by (i) the grain structure and texture, (ii) constituent particles, (iii) grain-boundary precipitates, (iv) tramp elements and (v) strain localization. Low fracture toughness has been attributed to the presence of tramp elements such as sodium, calcium, iron or sulphur [2] reducing the ductility, and in which sodium was found to be particularly potent to toughness reduction [3]. Constituent particles – being unavoidable in the production process of Al–Li alloys – are also sources of concern in fracture toughness (silicon-, copper- or magnesium-rich constituents) because they participate in the formation of voids at the particle–matrix interface [4]. Dispersoids added to Al–Li alloys act as grain-structure control agents and recrystallization inhibitors and, depending on particle–matrix interface details, they may play an unfavourable role during the fracture process. Similarly, crystallographic texture plays an important part in grain-boundary structure and deformation which may lead to anisotropic behaviour. Strain localization in Al–Li alloys, on the other hand, occurs by two very distinct mechanisms; one in which the deformation occurs preferentially in the ductile precipitate-free zone and the other by cutting through the shearable precipitate. The former has the aforementioned effect on fracture toughness, as it provides sites for nucleation of microvoids. In several binary Al–Li alloys, grain-boundary fracture was found to be associated with high volume fraction of shearable Al_3–Li (δ') precipitates [5]. Clearly these references show the importance of fracture properties and the concern as possible replacements for the conventional aluminium

0022–2461

alloys, in spite of being in favour of structural weight savings, density, strength, stiffness and damage tolerance.

In order to obtain good properties, microstructure, chemical composition, mechanical processing and heat treatment will play a crucial role, and although some of these relationships are not yet understood, the alloying elements of lithium, copper and magnesium appear to strengthen most Al–Li alloys due to both precipitation and solid-solution hardening. Without copper and magnesium, lithium forms coherent Al_3–Li (δ') precipitates which become sheared by dislocations and fail due to planar slip. For the alloy 8090, for instance, the main strengthening phase Al_3Li precipitates throughout the matrix during quenching. When copper and magnesium are present and when ageing takes place, S′(Al_2CuMg), T_1(Al_2CuLi) and T_2(Al_2CuLi_3) phases are precipitated, providing the barriers to dislocations and resulting in homogeneous deformation process. The grain-refining elements, in particular zirconium, reduce the grain size and improve ductility. But among all the elements listed earlier, iron is probably the tramp element which has the greatest effect on the fracture toughness in Al–Li alloys [6, 7].

The introduction of a hard precipitate or an inclusion can have a dramatic effect on mechanical properties as it tends to affect both the fatigue and fracture resistance of the composite. Hard inclusions when introduced into a soft matrix produce localized strain concentrations due to the mismatch of mechanical and probably physical properties. Thermal mismatch may generate residual stresses sufficient to deform the matrix plastically, setting up a large dislocation density which could accelerate the precipitation kinetics in the alloy [8]. This occurs during production or heat treatment of the metal matrix composite (MMC) as the cooling rates and the thermal expansion coefficients between the matrix and the reinforcement introduce both compressive and tensile residual stress fields. In general, the matrix is usually in tension while the reinforcement attains a compressive stress. At the interface between the matrix and the reinforcement, stress differentials occur which are locations of crack initiation. However, whether the reinforcement has a detrimental or beneficial effect on the deformation and fracture response depends on a number of factors such as processing method, reinforcement content, size and shape of particles and the heat treatment [8, 9]. Collaboratively, these factors will, for instance, determine both crack initiation life and propagation in fatigue but the mechanism of failure is strongly governed by the total response of the alloy's constituents to cyclic loading.

Failure mechanisms in MMCs are important at a microscopic level and range from reinforcement cracking, interface debonding between particles and matrix to progressive matrix damage [10]. These are all micro-damage processes and, in the case of crack initiation from reinforcement cracking, at least in Al–SiC_p systems, this mechanism is important only when the particle size is in excess of 20 μm [11]. The nucleation of cavities in the vicinity of the reinforcement will depend strongly on the nucleation event, promoted by a high level of triaxial constraint resulting from localization of the applied strain and from thermal contraction effects [12]. Progressive matrix damage, on the other hand, involves matrix slip and surface roughening which is shown to form intrusions and extrusions. The deformation and fracture response of the MMC thus strongly becomes a function of all combined effects but there is no way in which an overall conclusion can be derived from the role of the reinforcement. Moreover, there is some disagreement on the role of the reinforcement in influencing the fatigue crack growth resistance, as some studies suggest an increase in resistance, compared with the matrix, to crack growth [13, 14], others reported opposite results [15, 16].

The latter references indicate the complexity of interaction when a hard particle is introduced into a ductile matrix. An assessment of properties takes the form of tests in which the fracture toughness and fatigue crack growth in tension were the means of characterization. It then becomes relatively easy to determine under which conditions the MMC exhibits superior behaviour compared with the monolithic. Consider now the effects of deliberately introducing a stress field to a notch of the MMC and its subsequent cyclic loading under fully compressive loads. For some monolithic, mainly steels and aluminium alloys, the field of crack growth under cyclic compressive loading is reasonably established and the mechanism of crack initiation and propagation is also well documented. It is recognized that stable Mode I fatigue crack growth occurs in both ductile as well as brittle materials. When a notch, deliberately loaded in compression, is subsequently compressively cycled, crack growth occurs in the zone of residual tension. Crack propagation is fastest in the initial stages of cyclic loading but growth diminishes and falls to zero when the crack tip reaches the threshold of this stress field. The crack length and growth rate are found to be dependent on notch geometry, the initial value of preload, stress state, stress range and applied mean load [17–21].

The present work characterizes how the magnitude and form of the residual stress field modify the crack-growth behaviour and the range of the effective stress intensity, ΔK_{eff}, in the Al–Li alloy 8090 reinforced with SiC_p. Of particular interest in this work are the shape and magnitude of the residual stress field originated from the first compressive load and after crack initiation, crack advance and failure mechanism during cyclic loading. The cyclic stress range will be determined as demonstrated elsewhere [21] where the compliance analysis is used to infer the range of the effective driving force, ΔK_{eff}. A comparison is made considering the microstructure of the unreinforced Al–Li alloy which serves as the control alloy.

2. Experimental procedure

2.1. Material and specimen design

The MMC was produced by BP Research and supplied by RAE Farnborough in the form of 25 mm

TABLE I Mechanical properties of Al–Li alloys 8090 and 8090 reinforced with 17 vol % SiC particles

Alloy	UTS (MPa)	0.2% proof strength (MPa)	Strain to failure (%)	Modulus (GPa)	Density ($g\,cm^{-3}$)
8090-T6	485	415	6–8	80	2.54
8090-T6 + 17% SiC	540	450	3–4	103	2.66

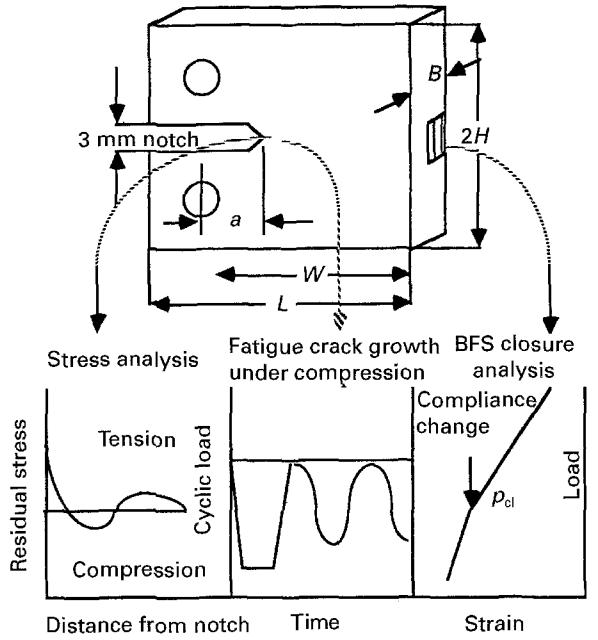

Figure 1 Specimen geometry and the experimental techniques used to determine the residual stress distribution and the stress intensity range, ΔK_{eff}, from compliance changes.

thick plates. It contained 17 vol % SiC particles with a mean particle size of 3 μm. The monolithic Al–Li alloy 8090 was produced by Alcan International Ltd, and the chemical analysis of the alloy was as follows (wt %): 2.42 Li, 1.15 Cu, 0.62 Mg, 0.09 Fe, 0.05 Si, 0.12 Zr, bal. Al. The chemical analysis of the MMC did not differ from that of the monolithic form. The mechanical properties are shown in Table I. Owing to the presence of the reinforcement, the strain to failure is approximately half that of the monolithic form. The present experiments employed compact tension specimens (CTS) with notches cut perpendicular to the rolling plane of the plate. The notch tip radius was 0.1 mm and a diagram of the geometry is shown in Fig. 1. A 120 Ω strain gauge attached to the back of the specimen normal to the plane of the notch was used in compliance measurements after fatigue crack growth and in the stress analysis of compressively preloaded notches.

2.2. Preloading and fatigue data

After polishing to 1/4 μm finish, specimens were preloaded compressively to 6 and 8 kN. The load was held for 30 s, and after unloading specimens were cyclically loaded in laboratory air under load control. Mean load level and amplitudes were selected so that the specimen always remained under compression, in the range of $-0.5\,kN \pm 0.5\,kN$. A sinusoidal waveform with a frequency of 20 Hz was used. All tests were carried out in duplicate. Crack length measurements were carried out *in situ* on the specimen surface with an optical travelling microscope which had a resolution of 0.02 mm. When the fatigue crack had ceased growing, crack closure measurements were carried out determining the change in slope of load versus back-face strain (BFS). These data were then used to define the effective part of the stress intensity range. For the precompression stress analysis, specimens were spark-eroded under paraffin oil emersion while recording changes in strain with increasing notch length. Cutting was stopped when the ligament reached the back of the specimen. The schematic in Fig. 1 shows the specimen geometry, experimental and analytical techniques used to determine compliance changes from fatigue testing and the residual stress field from precompression.

3. Results and discussion

Preloading in compression in notched CT specimens caused a plastic zone to form at the notch tip; on unloading, a tensile residual stress is developed in this region, biaxial at the surface and triaxial in the interior of the specimen. To study the residual stress field introduced from compressive preloading, two different routes may be followed utilizing the back-face strain (BFS) method which enables the compliance (the strain per unit load) to be used in the analysis. One route is by disturbing the stress field when cutting into the notch containing the non-uniform stress, and the other is by growing a fatigue crack which will also disturb the residual stress. In either case, the compliance will be changed when the notch or the crack is extended. The stress analysis related to the extension of the notch by cutting is now described.

3.1. Estimating the residual stress

The residual stresses induced in this test geometry by compressive preloading have been studied using a method first proposed by Reid [22]. It involves extending the notch by small increments with a spark erosion saw, while recording the changes in strain on the back-face of the specimen. After plotting BFS with notch length and fitting a fifth-order polynomial to this curve, the resulting coefficients are then used to analyse the stress field as a function of distance. The residual stress σ_R, is given by the following expression [22]

$$\sigma_R(t) = E\left(\frac{tg(t)}{2}\right) - 3t\int_t^T \frac{g(x)}{x}dx - \varepsilon(t) + \varepsilon(T) \quad (1)$$

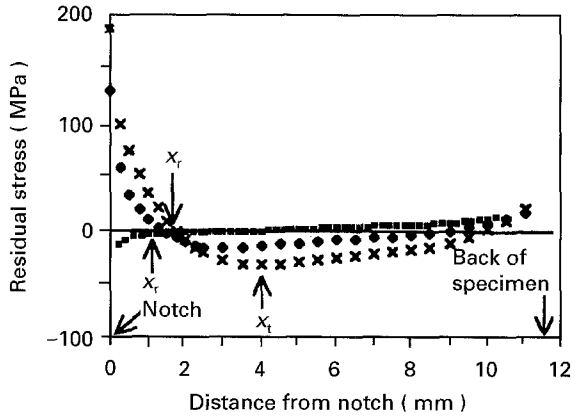

Figure 2 Variation of the residual stress distribution of alloy 8090 for (■) no preload and compressive preloads of (◆) − 6 and (×) − 8 kN.

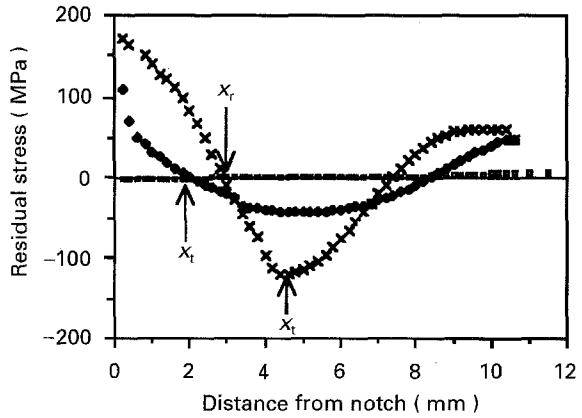

Figure 3 Variation of the residual stress distribution of alloy 8090 reinforced with 17 vol % SiC for (■) no preload and compressive preloads of (◆) − 6 and (×) − 8 kN.

where E is the Young's modulus, and the change in back-face strain during cutting is [$g(x)$, $\varepsilon(t)$ and $\varepsilon(T)$] and the distances x, t and T are defined in [21]. This equation is based on the assumption that during an increment of cutting the tensile residual stress over this increment is relaxed and this unbalances the remaining residual stress ahead of the notch tip. To restore the balance it is assumed that the uncut (uncracked) section of the specimen undergoes pure linear bending, detected by the strain gauge.

Figs 2 and 3 show typical examples of how the residual stress varies with distance from the notch for specimens preloaded to two different levels of compressive load in addition to the control specimens without preloading. As expected, the magnitude of residual stress increases with the level of preload. The largest stress is found at the notch tip but falls rapidly with decreasing distance, x, until it reaches zero stress at a distance, x_r, from the notch. This is the original residual stress prior to cutting. When the notch is extended (either by cutting or by fatigue crack growth) this original residual stress distribution is modified, and the new stress at the tip of the notch falls beyond zero stress at a distance x_t from the original notch tip (where $x_t > x_r$) where stress values are now compressive.

The analysis of the control alloy indicates the original residual stress in the material without the introduction of a preload. The stress distribution with distance from the notch is seen as a maximum near the notch tip (− 22 MPa) and a compressive maximum at 5 mm; this distribution is expected and is in good accord with a number of results obtained in 2000 and 7000 series aluminium alloys [21, 23]. However, for both compressively preloaded specimens a tensile gradient is seen near the notch tip. The largest tensile stress gradient is obtained for the biggest preload of − 8 kN. The values of x_r and x_t (the distances of zero stress and maximum compressive stress, respectively) as well as the control sample are given in Table II. It is seen that these distances are a function of the magnitude of the residual stress field; both distances increase with increasing magnitude, that is with increasing value of the pre-load (− 8 kN > − 6 kN).

As shown in Fig. 3 the residual stress field for the reinforced alloys is similar to the unreinforced alloy only as far as the shape of these distribution curves is concerned. For the control alloy (without preload) the reinforcement has no noticeable effect on shape and magnitude of the residual stress distribution. For specimens compressively preloaded to − 6 and − 8 kN, the notch tip stresses are smaller but a larger stress field can be produced compared with that in the unreinforced alloy preloaded to identical load levels. As a result the critical tensile and compressive stress levels for distances x_r and x_t are increased and as will be shown, most crack growth occurred within the region of tensile residual stress, $x \leqslant x_t$ due to the presence of the reinforcement (see also Table II for analysis of data). The model introduced later in Fig. 7 will discuss the underlying features of the MMC for the increase in tensile distance from the notch.

TABLE II Values of residual stress, σ_{Rmax} and σ_{Rmin} and positions of zero stress, x_r and x_t, calculated from results of the cutting experiment

Alloy/preload F_0 (kN)	σ_R (1st max) (MPa)	σ_R (min) (MPa)	x_r (mm)	x_t (mm)	σ_R (2nd max) (MPa)
8090					
no preload	22.0	− 10.3	0.20	–	–
− 6	132.8	− 15	1.15	3.00	17.7
− 8	188.1	− 30	1.80	4.00	23.4
8090 RE					
no preload	–	− 6.40	2.60	–	–
− 6	108.5	− 43.4	2.10	5.00	48
− 8	171.4	− 120	2.88	4.60	72

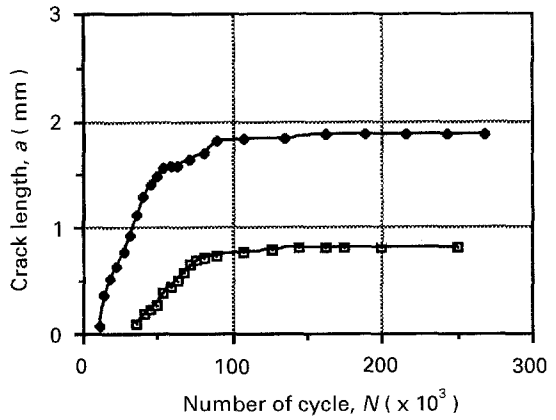

Figure 4 Crack length a versus number of cycles N of unreinforced alloy 8090 for compressive preloads of (⊡) − 6 and (◆) − 8 kN.

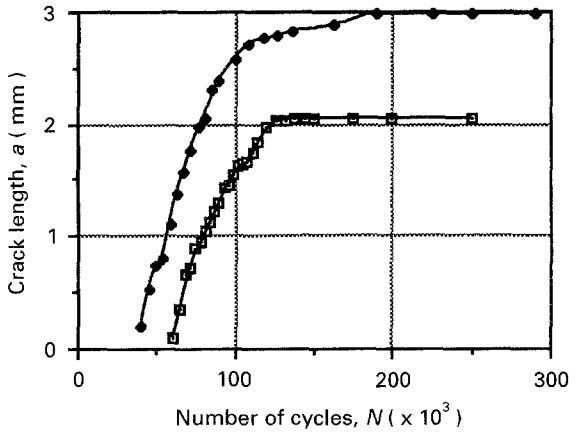

Figure 5 Crack length a versus number of cycles N of the reinforced alloy 8090 for compressive preloads of (⊡) − 6 and (◆) − 8 kN.

Further analysis of Figs 2 and 3 indicates that the distribution of residual stress over the remaining ligament must retain equilibrium, that is to say that the negative and positive areas under the stress versus distance curve should be equal. It is also seen from these figures and Table II that there are two tensile peaks in each curve, one near the notch (termed $\sigma_{R(1\,max)}$) and the other towards the back of the specimen (termed $\sigma_{R(2\,max)}$). For both the unreinforced and reinforced alloys and values of increasing compressive preload of 6 and 8 kN, the areas were found between 48%, 43%, 47% and 53% respectively, or an imbalance between tension and compression forces between 4% and 14%. These values suggest that the model used is satisfactory in estimating the magnitude of residual stresses and is in good agreement with the generally accepted view of the stress distribution around notches.

3.2. Crack-growth rates and effective stress intensity range

Identically preloaded specimens as used in the stress analysis work are also employed in the fatigue crack growth experiments. The results for the unreinforced alloy are presented in Fig. 4 and those for the reinforced alloys in Fig. 5, preloaded to − 6 and − 8 kN. The following discussion applies to Fig. 4. After a short number of "incubation" cycles a crack is nucleated at the root of the notch. Although not shown in these graphs, the initial crack growth for both preloads occurred at an accelerating rate due to an increase in stress intensity accompanying a transition from a physically small to a long crack. As was shown by Smith and Miller [17] the crack must out-grow a notch-zone effect with a length of $[0.13(D\rho)^{0.5}]$ where D is the notch length (9.5 mm) and ρ is the root radius (0.1 mm). The crack length was estimated to be 0.124 mm which is in good agreement with the region of observed crack growth. Subsequent crack growth rates were fastest but growth eventually fell and stopped altogether. In both cases it is seen that the final crack length increased with the value of the initial preload and because the applied mean loads were identical in all specimens, the effect of an increased crack length is entirely due to the extent of the tensile stress field introduced from the initial preload. Fig. 5 shows the dependence of crack length with number of cycles as a function of preload in the reinforced alloy. As in Fig. 4, the same discussion applies to Fig. 5 except for the following different features: (a) the number of "incubation" cycles has increased for each preload. As in Fig. 4 the largest preload shows the shortest number of "incubation" cycles; (b) the initial slopes of each a versus N curve have increased steeply suggesting that the crack velocity has equally increased; and (c) the final crack length has also increased and is a function of preload and an effect of reinforcement.

The dependence of the final crack length on preload can be explained in the following way. Two "plastic zones" are formed in the static and cyclic loading sequence, see Fig. 9 for explanation. One is the notch field plastic zone formed from the process of preloading [17] which gives rise to the tensile residual stress field and the other is the cyclic plastic zone at the crack tip formed during fatigue. The superimposed cyclic applied stress field is solely responsible in propagating a crack. This is because crack growth depends on the stress intensity range and growth will cease when the stress intensity range, ΔK, at the crack tip falls to the threshold value, ΔK_{th}. Because ΔK depends on the cyclic change in crack opening which in turn depends on the sum of the (static, tensile) residual stress field and the (cyclic compressive) applied stress field, it follows that the final crack length increases with both the cyclic and plastic zone size, that is with increases of preload. An evaluation of the range of the effective stress intensity, ΔK_{eff}, is now described.

Optical examination of the side surfaces of fatigued specimens confirmed that the cracks appeared to be gaping. By applying a compressive load to the open crack of the specimen, the measured compliance as shown in Fig. 6 can be used to find the load over which the crack is open, that is where the compliance changes from a non-linear to a linear slope. This approach to finding the closure load is identical to that described elsewhere [21, 23]. The effective stress intensity range, ΔK_{eff}, is determined by finding the

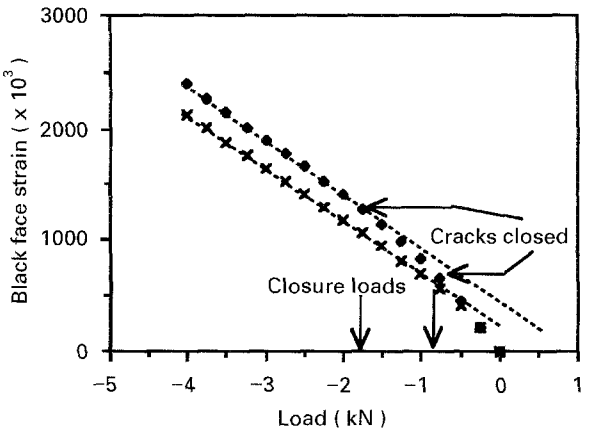

Figure 6 Compliance graph of BFS plotted against compressive load to determine crack closure load for cracks (×) 2.05 and (◆) 3.01 mm in length.

effective closure load range, ΔF_{eff}, for a given stress field, i.e.

$$\Delta F_{eff} = F_{max} - F_{min} \text{ or } (F_{max} - F_{cl}) \quad (2)$$

where F_{max} is the maximum applied load, F_{min} is the minimum applied load, and F_{cl} is the measured closure load. The value of ΔK_{eff} is taken as the smaller of $(F_{max} - F_{min})$ and $(F_{max} - F_{cl})$ provided this is positive. As seen from Fig. 6 for the graph of the -8 kN preload, closure loads are larger or above the minimum load in the fatigue cycle (they are outside the cyclic fatigue loading range), hence this crack is fully open between F_{max} and F_{min}. However, for the unreinforced and the reinforced specimens preloaded to -6 kN, a fraction of the closure load lies within the fatigue loading range, hence this part is closed and does not contribute to crack opening and growth. The effective stress intensity range, ΔK_{eff}, near the notch tip is then calculated using the equation [24]

$$\Delta K_{eff} = \frac{Y \Delta F_{eff}}{BW^{1/2}} \quad (3)$$

where Y is a dimensionless function of a, the crack length, W is the ligament length from the load line to the back face of the specimen, and B is the thickness.

3.3. Comparison and analysis of data from cutting and fatigue

The analysed data suggest that the initial stress field at the notch may be taken as being approximately equivalent to the value of the closure load if the specimen is loaded in tension. The residual stress falls to zero at a distance x_r when the crack stopped growing. As seen from Table II for identical initial stresses at the root of the notch, the reinforced alloys produced much larger x_r distances compared with the stress fields in the unreinforced alloy. There was generally good agreement of these distances with those obtained in the fatigue experiments, although x_r distances for the unreinforced alloy from the stress analysis appeared to be slightly bigger, whereas the opposite is the case for the reinforced alloy. It is suggested that the residual stresses redistribute when the crack starts growing and as a result move x_r to a slightly larger distance from the notch, probably between x_r and x_t. For the reinforced alloys preloaded to -8 kN, this is found to be the case, because cracks grew in excess of the x_r values computed from the stress-field analysis, see also Table III. Taking into account the analysis of the stress distribution from the cutting experiments and the growth behaviour of these alloys, it is obvious that most of the crack growth occurred within the region of *tensile* residual stress. A similar conclusion was reached for the growth behaviour of an aluminium alloy of the 7000 series subjected to similar cyclic compressive loading [21].

The preload levels as given in Table III exhibit the effective stress intensity range for a given stress field. For the unreinforced alloy at both preload levels, closure was only detected for the specimen preloaded to -6 kN, hence the effective crack opening force, ΔF_{eff}, is smaller than for the specimen preloaded to -8 kN. In the latter case it is assumed that all fatigue amplitude corresponded to full opening and growth of the fatigue crack, see also Fig. 6. It is seen that all closure values in this alloy are larger than P_{min} of the mean load (they lie outside the range of the fatigue amplitude), hence the crack will be fully open during the fatigue cycle. This table demonstrates that the reinforcement has a marked effect on both crack growth and closure of these alloys but additionally is strongly a function of tensile stress distance, x_r. Cracks without closure grew at an initial ΔK_{eff} of ~ 6 MPa m$^{1/2}$ and those partially closed at a slightly lower ΔK_{eff}, of 4.74 and 5.22 MPa m$^{1/2}$. These data are well above the fatigue threshold for the unreinforced 8090 alloy which is ~ 4 MPa m$^{1/2}$.

3.4. Stress distribution after fatigue crack growth

The relaxation of the residual stress in the notch region is now examined when a fatigue crack is growing

TABLE III Final crack length, initial crack growth rates and the effective stress intensity, ΔK_{eff}, calculated from closure measurements

Preload/ alloy	Final crack length (mm)	da/dN (10^{-8} m cycle^{-1})	F_{cl} (kN)	F_{max} (kN)	F_{min} (kN)	ΔF_{eff} (kN)	ΔK_{eff}, Eq. 2
8090							
−6	0.82	1.58	−0.80	0	−1.0	0.80	4.74
−8	1.78	3.33	−2.25	0	−1.0	1.00	5.93
8090 RE							
−6	2.05	3.54	−0.88	0	−1.0	0.88	5.22
−8	3.01	4.05	−1.75	0	−1.0	1.00	5.93

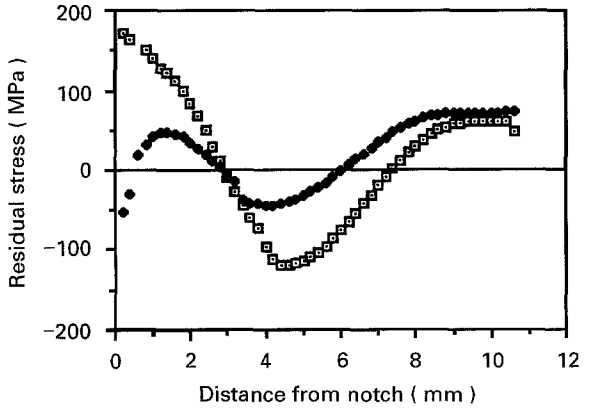

Figure 7 The original stress (□) and changes in residual stress distribution for (◆) a crack of 1.50 mm in length in the reinforced alloy 8090, both preloaded to 8.0 kN.

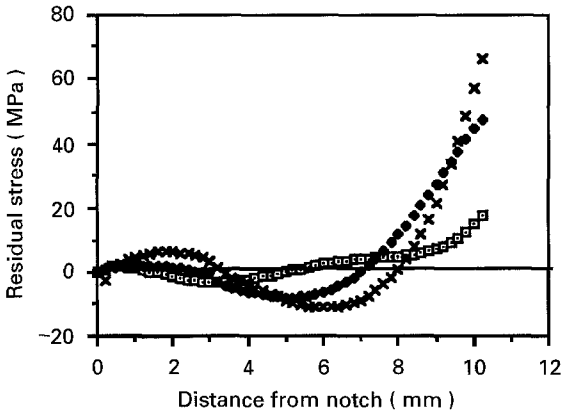

Figure 8 Variation of the residual stress for fully arrested cracks of (□) 0.82 and (◆) 2.06 mm crack length for the monolithic and for a crack of (×) 2.05 mm for the composite alloy 8090.

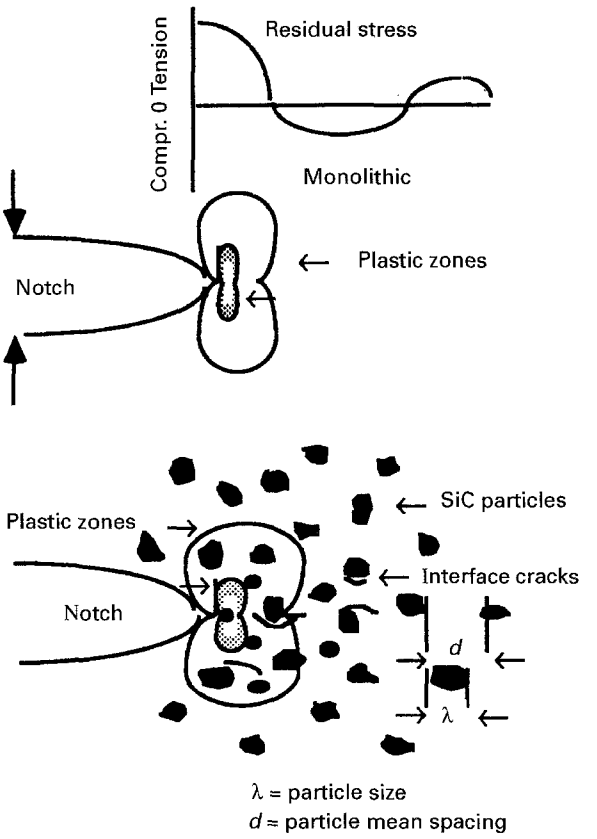

Figure 9 A model which explains the increase in tensile stress observed after precompression of the composite alloy 8090.

partially or fully through it. In Fig. 7 the stress distribution for notches preloaded to − 8 kN is analysed. The stress distribution as shown in Fig. 3 is the original stress prior to fatigue, revealing a non-linear stress distribution between the tensile maximum at the root of the notch up to a distance x_r of 3.0 mm from the notch. When a crack is grown compressively to a distance of 1.5 mm from the notch and a stress analysis is carried out, the resulting distribution curve in Fig. 7 shows quite clearly that the original large stress gradient is reduced to stresses of about 50 MPa at a distance of 1.5 mm. Because there is still sufficient residual stress left in the surrounding crack-tip region, this crack would continue to grow under cyclic compression until it reached the distance x_r (3 mm) of zero stress. For completely arrested cracks as shown in Fig. 8, the analysis reveals that crack growth has changed the initial stress field from highly tensile to almost zero stress, at least over the existing distance of high stress gradient. All stresses are relaxed in this region; they become slightly compressive at the mid-distance from the notch and tensile towards the back of the specimen. It is noted that the stress distribution towards the back of the specimen becomes strongly influenced by the original stress field in the notch region (see also Fig. 2 and Table II). The observation made in a photoelastic study [25] that the stress field is not disturbed when a crack was grown through it must be taken as questionable and cannot be supported taking the present results into account.

3.5. Increase of residual stress field in the MMC

The stress analysis in Figs 2 and 3 is summarized in Table II. It is seen that two similar stress levels are obtained at the root of the notch, taken in comparison with the monolithic form. However, the tensile distance of the reinforced specimens is significantly larger than that of the monolithic form and Fig. 9 provides a model of the analysis of Table II. Consistent with previous descriptions, preloading in compression causes plastic deformation at the notch and on unloading a tensile residual stress is developed because of the elastic springback of the material some distance away from the notch. This is identical for both the monolithic as well as the reinforced alloy and, as shown in Fig. 9, the extent of this residual stress is depicted by the distance from the notch enclosed by the plastic zone. Crack growth will cease when the crack reaches the boundary of the plastic zone which is equivalent to the distance x_r (see Table II) and almost identical with the observed final crack length given in Table III and Fig. 5. The entire stress field in the notch tip is governed by the deformation process of the matrix during compressive preloading and unloading.

For the reinforced alloy an additional loading effect takes place in the notch-tip region. The matrix

responsible for the elastic springback setting up tensile residual stresses initially provides the strain that will modify the existing stress field in and around the reinforcing particles. Despite the limited ductility of the reinforced alloy, stresses local to the reinforcement particles will become very large for modest plastic strains. This is accompanied by the development of a large reinforcement/matrix misfit which generates additional high levels of internal stresses. As plastic deformation of the matrix takes place during loading this must be matched by an elastic distortion of the reinforcement. Hence a larger plastic distortion must result (depicted as the enlarged plastic zone in Fig. 9) but there is a limit to the size of the plastic distortion in MMCs as the development of residual stresses will become limited due to stress relaxation. It is clear that as mismatch becomes larger the tendency for relaxation increases.

All relaxation processes are associated with the reduction in the overall energy of the stress field and this could be achieved by the development and growth of cracks. Cracks may be developed in the matrix manifested as matrix cavitation, fracture of the reinforcement or at the interfaces between the matrix and the reinforcing particles. Prior to fatigue, small cracks have been found after unloading, hence some relaxation is already achieved, but by far the greatest change occurs during *cyclic* compressive loading. This may also explain why the stress maximum at the root of the notch in the reinforced specimens was always smaller compared to the monolithic form. Because the mentioned processes of relaxation affect the load-bearing capacity of the MMC it is important to understand these mechanisms in which yield strength, failure strain, mean stress, particle size and mean spacings of the reinforcement phase all play their part [26].

3.6. Fracture morphology

The following observation applies equally to both the monolithic as well as the reinforced alloys. Fatigued specimens were broken open after crack closure determinations to examine their fracture morphology by light optical microscopy. Fig. 10 reveals the fracture appearance obtained light-optically for the reinforced alloys, where it is seen that almost all fatigue cracks appeared straight with little crack-front bowing between the interior and the surface region. This micrograph also shows the extent of crack-length increase with increasing compressive preload for the reinforced alloys. Fig. 10a is a typical fracture appearance of the specimen preloaded to -6 kN, while Fig. 10b is that for the preload of -8 kN. On both fracture surfaces a uniform morphology is observed starting from the notch (at the bottom) to the end of the crack tip. The overall shape of the crack front between the surface region and the interior suggests that the residual stress set up by preloading extended to a slightly greater distance from the notch at the surface than at the interior. This is because of the constraints on yielding which prevail at the surfaces compared with those of the interior, due to the larger plastic zones near the surfaces.

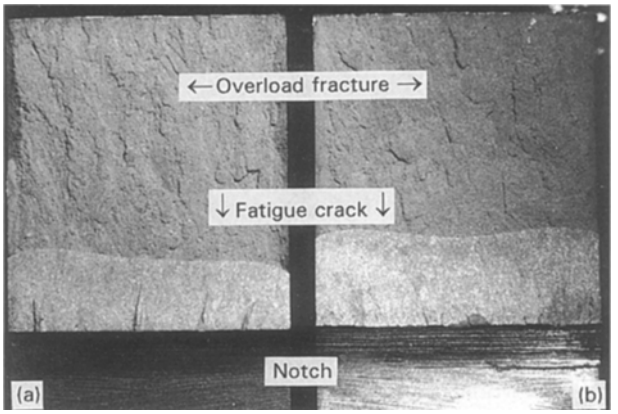

Figure 10 Final crack-tip profile and fracture morphology of the reinforced alloy 8090 after breaking open CT specimens, (a) -6 kN and (b) -8 kN preload; $\times 5.1$.

Scanning electron microscopy (SEM) revealed a varied fracture mode dominating more than half the fracture surface. No surface contact damage was observed on specimens where closure loads were larger than the minimum fatigue loads, but for specimens where the closure loads were less than the minimum fatigue loads, occasional surface contact was seen. The morphologies observed varied from flat transgranular, intergranular to isolated pockets of ductile dimpled fracture appearance, but there was no discernible appearance between the monolithic and the reinforced alloys.

4. Conclusions

Al–Li alloys unreinforced and reinforced with SiC_p, in form of notched CT specimens, were examined by subjecting them to a deliberate compressive preload. The developed stress fields were analysed by stress analysis and fatigue experiments under cyclic compressive loading and these results are summarized below.

1. After compressive preloading and unloading of a notch a tensile residual stress field was formed at the root of the notch and an estimate of the stress distribution was obtained. In both the monolithic and the MMC, stresses were tensile and varied with distance.

2. Residual stresses in the reinforced alloy were found to be larger than those in the monolithic form; this was due to the presence of the reinforcement particles which increased the mismatch stress at the interface of SiC particles and the matrix.

3. Fatigue crack experiments conducted under cyclic compressive loading supported the results obtained from stress analysis. The final crack length increased with increase in preload (and tensile stress) but longer cracks were grown in the MMC because of an increased residual stress field.

4. Using a method of compliance, crack closure loads were determined allowing an estimate of the effective driving force, ΔK_{eff} over which crack growth occurred. It was found that most crack growth occurred over a distance in the region of tensile residual stress.

5. The stress analysis of cracks grown over different crack lengths indicated that the residual stresses are relaxed and fall to lower levels of stress. For non-propagating cracks, the entire stress field falls to zero at distances over which the stresses were originally tensile.

Acknowledgements

The author thanks D. L. Bartlett, RAE Farnborough, for the supply of the reinforced MMC and discussion on heat-treatment, P. Ledgard and R. Black of the Materials Discipline for machining the MMCs, and also the Materials Department at the Open University for the use of all other facilities.

References

1. E. S. BALMUTH and R. SCHMIDT, in "Proceedings of the 1st International Conference on Aluminium–Lithium Alloys" (The Metallurgical Society of AIME, Warrendale, PA, 1981) p. 69.
2. E. A. STARKE Jr, T. H. SANDERS Jr and I. G. PALMER, *J. Metals* **38** (1981) 24.
3. K. T. V. RAO and R. O. RITCHIE, *Mater. Sci. Technol.* **5** (1989) 882.
4. N. J. OWEN, D. J. FIELD and E. P. BUTLER, in "Proceedings of the 3rd International Conference on Aluminium–Lithium Alloys III", July 1985, edited by C. Baker, P. J. Gregson, S. J. Harris and C. J. Peel (Institute of Metals, London, 1986) p. 576.
5. T. H. SANDERS Jr and E. D. STARKE Jr, *Acta Metall.* **30** (1982) 927.
6. C. J. PEEL, B. EVANS, C. A. BAKER, D. A. BENNET, P. J. GREGSON and H.M. FLOWERS, in "Proceedings of the 2nd International Conference on Aluminium–Lithium alloys", July 1984, edited by T. H. Sanders and A. E. Starke (The Metallurgical Society of AIME, New York, 1984) p. 363.
7. S. SURESH and K. K. CHAWLA, in "Fundamentals of Metal-Matrix Composites" (Butterworth-Heinemann, Stoneham, MA, 1993) p. 251.
8. W. A. LOGSDON and P. K. LIAW, *Eng. Fract. Mech.* **24** (1986) 737.
9. S. S. YAU and G. MAYER, *Mater. Sci. Eng.* **82** (1986) 45.
10. M. MANOHARAN and J. J. LEWANDOWSKI, *Acta Metall. Mater.* **38** (1990) 486.
11. D. LLOYD, *ibid.* **39** (1991) 59.
12. A. J. PADKIN, M. F. BERETON and W. J. PLUMBRIDGE, *Mater. Sci. Technol.* **13** (1987) 217.
13. T. CHRISTMAN and S. SURESH, *Mater. Sci. Eng.* **102** (1988) 211.
14. D. L. DAVIDSON, *Eng. Fract. Mech.* **33** (1989) 965.
15. S. KUMAI, J. E. KING and J. F. KNOTT, *Fat. Fract. Eng. Mater. Struct.* **13** (1990) 511.
16. S. SURESH, in "Fatigue of Materials" (Cambridge University Press, Cambridge, 1991) p. 252.
17. R. A. SMITH and K. J. MILLER, *Int. J. Mech. Sci.* **19** (1977) 11.
18. C. N. REID, K. WILLIAMS and R. HERMANN, *Fat. Eng. Mater. Struct.* **26** (1979) 26.
19. N. A. FLECK, C. S. SHIN and R. A. SMITH, *Eng. Fract. Mech.* **21** (1985) 173.
20. D. K. HOLM, A. F. BLOM and S. SURESH, *ibid.* **23** (1986) 1097.
21. R. HERMANN, *Fat. Fract. Eng. Mater. Struct.* **17** (1994) 93.
22. C. N. REID, *Scripta Metall.* **22** (1988) 451.
23. R. C. KU and M. A. POMPETZKI, in "Mechanics of Crack Closure" ASTM STP 982 (American Society for Testing and Materials, Philadelphia, PA, 1988) p. 171.
24. ASTM Standard E-399 (American Society for Testing and Materials, Warrendale, Philadelphia, PA, 1992).
25. R. P. HUBBARD, *Trans. ASME J. Basic Eng.* (1969) 625.
26. R. HERMANN, unpublished work (1994).

Received 14 October 1994
and accepted 20 January 1995